LETTER

Reply to Subramaniam, van Heel, and Henderson: Validity of the cryo-electron microscopy structures of the HIV-1 envelope glycoprotein complex

Subramaniam (1), van Heel (2), and Henderson (3) express their opinions and hypotheses about our cryo-electron microscopy (EM) structures of the uncleaved HIV-1 envelope glycoprotein [Env(-)ΔCT] trimer (4, 5). There are no data in these communications, nor elsewhere in the published literature, that contradict our results; however, we conducted systematic additional studies that provide strong evidence disproving their hypotheses. We appreciate the potential pitfalls of analyzing low-contrast images and indeed took specific measures to avoid reference bias in our particle-picking approach (6). Importantly, we conducted validation studies on our Env(-)ΔCT structures using independent datasets and tests. We offered the primary data to the reviewers of this communication. We respond to the comments of Subramaniam, van Heel, and Henderson as follows.

Comment 1: There Are No Env(-)ΔCT Particles in Our Micrographs—Our Picked Particles Represent Pure Noise That Was Aligned to Recreate the Reference Used in our Particle-Picking Approach

In single-particle cryo-EM, a tradeoff exists between the contrast of the specimen image and the achievable resolution (7). To allow determination of the Env(-)ΔCT structure at optimal resolution, a large number of closer-to-focus, low-contrast images from focal pairs were analyzed. The signal-to-noise ratio (SNR) of our particles is comparable to those used in other cryo-EM studies that sought to maximize resolution; we deposited a set of original micrographs in the Electron Microscopy Data Bank to allow investigators to evaluate the raw data (8). Subramaniam's and Henderson's comparisons of our dose-limited micrographs with their overdosed particle images (1, 3) are misleading; to achieve high contrast in their examples, high-resolution information in those overdosed images is sacrificed as a result of excessive radiation damage.

We devised an approach to select and validate particles from low-contrast images that is sensitive, yet avoids reference bias from the particle-picking template (6). In this dual-target function validation approach, fast local correlation with a low-resolution template was used for automated particle picking (9), followed by particle verification through maximum-likelihood (ML) image alignment (10, 11) (Fig. 1*A*). The log-likelihood function used in ML alignment is not equivalent to the fast local correlation function, such that any reference bias that occurred in the particle-picking procedure can be removed through ML alignment. This allows true signal to be verified no matter what type of template is used for particle picking (6). By using different target functions for particle selection and particle verification, the probability that both functions become trapped in the same local optimum is infinitesimally small. Control experiments testing Subramaniam's, van Heel's, and Henderson's speculations that we aligned pure noise to achieve our reconstruction of the Env(-)ΔCT trimer with the dual-target function approach failed to support their hypotheses (Fig. 1*B*). Even when the fast local correlation picked pure noise images to recapitulate the particle-picking template [i.e., to produce a "head of Einstein" or a projection view of the Env(-)ΔCT trimer], the influence of the particle-picking template on the ML alignment is either not observable (if starting from a Gaussian circle or a pure noise image as reference) or diminishes and disappears with refinement (if starting from the particle-picking template; Fig. 1*B*). Thus, because there is no real Einstein in the pure noise images, the converged ML alignment indicates the absence of Einstein, as expected (6). These experimental results directly contradict van Heel's hypotheses that "because the reference bias is introduced at [an] early stage, it becomes irrelevant that the projection classes can be averaged without using further references or symmetry assumptions," and that "...the well-defined secondary structure in the final map...appears to have come from reiterating their reference-based particle-picking procedures..." (2). Additional details of our particle-picking approach, with more examples of the ability of ML alignment to verify true particles and resist reference bias, are available in the arXiv preprint online database (6).

Alignment of pure noise does not allow the extraction of structural information that is of higher resolution than that which is present in the reference model (12). van Heel uses our 11-Å structure (Electron Microscopy Data Bank, accession no. EMD-5418) to pick and average 670,000 particles from random noise, and the unaligned class averages were used to reconstruct a density map that cross-correlated with the reference to a resolution of 13 Å. van Heel avoided image alignment and did not attempt to refine this 13-Å map; it has been well established that the resolution of maps generated by model bias from pure noise does not improve and can become much worse with refinement (12). Based on our results (Fig. 1 *B*, *2*), van Heel's artifactual reconstruction from pure noise could not be reproduced by ML refinement. The lack of resolution improvement and failure of refinement in van Heel's example clearly contrasts with our ML refinement of the Env(-)ΔCT structure, starting from a featureless geometric shape or a 60-Å reference and proceeding to higher-resolution structures (Fig. 1*D*). In summary, the oversimplified procedure that van Heel used to generate his pure noise reconstruction cannot legitimately be likened to our reconstruction and refinement, as both the procedures and the datasets differed.

Subramaniam, van Heel, and Henderson refer to our use of a "3D structure" or "molecular model" as a reference. Because these terms are ambiguous and might be misinterpreted, we emphasize that we used only featureless geometric shapes or appropriately low-pass-filtered cryo-EM density maps as references in the structure refinement.

Author contributions: Y.M., L.R.C.-M., and J.G.S. designed research, performed research, analyzed data, and wrote the paper.

The authors declare no conflict of interest.

[1]To whom correspondence should be addressed. E-mail: joseph_sodroski@dfci.harvard.edu.

Comment 2: Env(-)ΔCT Structures Lack Validation

Henderson discusses validation tests for cryo-EM structures, and notes that the controversial inositol triphosphate receptor (IP3R) structure "has been fully validated by recently introduced tests" (3, 13). We note that each of these criteria for validation of the IP3R structure (13) has now been met by our work with the Env(-)ΔCT structure:

i) Correspondence between the computed projections of the reconstructed Env (-)ΔCT map and the ML-aligned class averages. See figure S4 of ref. 4.

ii) Tilt-pair validation. We recently collected higher-contrast images of an independent preparation of the Env(-)ΔCT trimer at two tilt angles and calculated a tilt-pair parameter plot (14, 15) (Fig. 1*C*). The clustering of the calculated particle orientations around the experimental tilt axis and tilt angle supports the validity and handedness of our Env(-)ΔCT reconstruction.

iii) Comparative refinement with different reconstruction methods. Use of a different algorithm to analyze the same dataset can provide information on the reliability of the reconstruction up to a given resolution level. Independent subsets of the Env(-)ΔCT data were analyzed using RELION, which uses a 3D ML approach and incorporates gold standard refinement to minimize noise bias in the reconstruction (16). Using a 100-Å geometric shape with threefold symmetry as a reference to analyze a 9,993-particle dataset yielded a 20-Å RELION reconstruction (Fig. 1 *D*, *1*). Repeating the RELION reconstruction with an independent 124,478-particle dataset, starting from a 60-Å reference, yielded a 10-Å RELION reconstruction (Fig. 1 *D*, *2*). Both RELION reconstructions are consistent with each other and with our published Env(-)ΔCT maps (4, 5).

iv) Gold standard resolution estimation (5). The value of the gold-standard approach in minimizing the introduction of noise into the reconstruction is not diminished by the use of the same low-resolution initial reference (17, 18). After convergence, to reduce the contribution of the poorly ordered distal glycans to the reconstruction, we applied a mask, which was created by dilating the lowest molecular contour surface of the refined map by ~20 Å, for an additional five rounds of refinement. This did not change the protein component of the map, but allowed clearer localization of the peptide-proximal glycan stalks (5). As noted above, the published Env(-)ΔCT map (5) is consistent with two independent RELION reconstructions of the Env(-)ΔCT structure, which did not use a mask in the refinement (Fig. 1*D*).

These results support our assertions that our picked particles represent bona fide Env(-)ΔCT trimers and that the SNR of the images is sufficient to obtain reliable structural information about the trimer. Details of these additional validation studies will be reported elsewhere, which will be accompanied by public release of a full particle dataset used in the RELION reconstruction. The primary evidence for the validity of our Env(-)ΔCT structures was included in the published papers (4, 5):

v) Excellent rigid-body fit of the X-ray crystal structure of the conformationally invariant gp120 outer domain into the cryo-EM map (figure 2 *A* and *B* in ref. 5).

vi) Appearance of secondary structural features in the density maps at the expected resolution (5).

vii) Correspondence between the location of stalks of nonprotein density and known sites of *N*-linked glycosylation (figure 5 of ref. 5).

viii) Correspondence with tomograms of the native Env spikes on virions (figure 6 in ref. 4).

ix) Prediction of the HIV-1 neutralizing potency of a panel of antibodies directed against the receptor-binding site of gp120 (figure 6 in ref. 5).

Response to Specific Technical Comments

Subramanian argues that there is no correlation beyond 20 Å in the Fourier shell correlation (FSC) between our 6- and 11-Å maps. He then concluded that the two maps are inconsistent. This is not true. By adding a critical FSC (calculated from the two maps) to the cross-map FSC, one can see that there is clear correlation above the critical FSC up to ~11 Å (Fig. 2*A*). FSC estimates of resolution are known to be quite sensitive to statistical bias due to differences in the numbers of particles and the experimental sources of the images used in the two reconstructions (7). The result is that the FSC-0.5 cutoff often underestimates the correlation between maps generated from statistically uneven datasets. This is why useful FSC resolution assessment is best done between maps of evenly split half datasets. When this condition is not met, one can resort to the critical FSC to assess the actual correlation between maps generated from different experiments. Subramanian's assumption that the filtered 6-Å map and the 11-Å map should be identical also ignores the fact that certain surface features (e.g., glycans) can only be detected at higher levels of resolution by analyzing a larger dataset.

Subramanian argues that the Env(-)ΔCT structures do not agree with the cryo-electron tomography map (EMD-5019) of the native, cleaved Env trimer (19) in the gp41 transmembrane region. He claims that EMD-5019 represents only the Env ectodomain, yet several of his own publications show the gp41-associated density extending into the membrane (19–21). In figure 1 *D*, *E*, and *G* of ref. 1, Subramanian misaligned our Env(-)ΔCT density maps with respect to the membrane in support of his arguments. We present the correct alignment of our Env(-)ΔCT maps in Fig. 2*B*. We estimate the hydrophobic thickness of the lipid bilayer to be ~30 Å and note that the lengths of the proposed gp41 transmembrane helices are sufficient to traverse the membrane. Higher-resolution information will be required to determine unambiguously the location of the membrane relative to the HIV-1 envelope glycoprotein structure.

Subramanian finds it surprising that the most ordered regions of our 6-Å density map are the gp41 transmembrane helices and the gp120 V4 loop, which he believes is disordered in crystal structures of monomeric gp120. In contrast to his statement, the V4 loop was completely resolved in a crystal structure (Protein Data Bank ID code 2B4C) of gp120 from the JR-FL strain of HIV-1 [the same strain from which the Env(-)ΔCT glycoprotein used in our studies was derived] (22). There is no obvious reason to question the existence of structural order in the left-handed coiled coil formed by the gp41 transmembrane helices.

Henderson believes that a circle of dark density that surrounds the edge of the particle averages "should not be present in the raw images so must arise from masked projections from the 3D map or model used to extract the single particles" (figure 3 *G* and *H* of ref. 3). The features that Henderson describes in the particle averages are commonly observed when the normalization procedure in the XMIPP program (23) is used. See figure 2*B* in ref. 10 for another example. Therefore, Henderson's speculative explanation that the dark circle arose from

masked projections of a 3D map or model is unnecessary and incorrect. We also note that the signals in figure 3 *G* and *H* of ref. 3 are consistent with real particle averages and inconsistent with noise aligned to a template, contradicting Henderson's statement that he found no evidence for particles in our data.

Henderson asserts that the final 6-Å map of the Env(-)ΔCT trimer "shows prominent radial density streaks, which are often due to overfitted noise." We agree that overfitted noise could appear as density radiating from a common center. However, unlike overfitted noise, the density in the 6-Å map does not radiate from a common center. As shown in figure 4*C* of ref. 5, the so-called "radial density streaks" form triangular shapes, and no common center exists for these streaks.

Youdong Mao[a], Luis R. Castillo-Menendez[a], and Joseph G. Sodroski[a,b,c,1]

[a]Department of Cancer Immunology and AIDS, Dana-Farber Cancer Institute, Department of Microbiology and Immunobiology, Harvard Medical School, Boston, MA 02115; [b]Department of Immunology and Infectious Diseases, Harvard School of Public Health, Boston, MA 02115; and [c]Ragon Institute of MGH, MIT and Harvard, Cambridge, MA 02139

1 Subramaniam S (2013) Structure of trimeric HIV-1 envelope glycoproteins. *Proc Natl Acad Sci USA* 110:E4172–E4174.
2 van Heel M (2013) Finding trimeric HIV-1 envelope glycoproteins in random noise. *Proc Natl Acad Sci USA* 110:E4175–E4177.
3 Henderson R (2013) Avoiding the pitfalls of single particle cryoEM: Einstein from noise. *Proc Natl Acad Sci USA* 110:18037–18041.
4 Mao Y, et al. (2012) Subunit organization of the membrane-bound HIV-1 envelope glycoprotein trimer. *Nat Struct Mol Biol* 19(9): 893–899.
5 Mao Y, et al. (2013) Molecular architecture of the uncleaved HIV-1 envelope glycoprotein trimer. *Proc Natl Acad Sci USA* 110(30): 12438–12443.
6 Mao Y, Castillo-Menendez L, Sodroski J (2013) Dual target function validation of single-particle selection from low-contrast cryo-electron micrographs. arXiv:1309.2618[q-bio.QM].
7 Frank J (2006) *Three-Dimensional Electron Microscopy of Macromolecular Assemblies: Visualization of Biological Molecules in Their Native State* (Oxford Univ Press, Oxford).
8 http://www.ebi.ac.uk/~ardan/aspera/em-aspera-demo.html or contact Dr. Ardan Patwardhan (ardan@ebi.ac.uk).
9 Shaikh TR, Trujillo R, LeBarron JS, Baxter WT, Frank J (2008) Particle-verification for single-particle, reference-based reconstruction using multivariate data analysis and classification. *J Struct Biol* 164(1): 41–48.
10 Scheres SH, et al. (2005) Maximum-likelihood multi-reference refinement for electron microscopy images. *J Mol Biol* 348(1):139–149.
11 Sigworth FJ (1998) A maximum-likelihood approach to single-particle image refinement. *J Struct Biol* 122(3):328–339.
12 Shaikh TR, Hegerl R, Frank J (2003) An approach to examining model dependence in EM reconstructions using cross-validation. *J Struct Biol* 142(2):301–310.
13 Murray SC, et al. (2013) Validation of cryo-EM structure of IP$_3$R1 channel. *Structure* 21(6):900–909.
14 Rosenthal PB, Henderson R (2003) Optimal determination of particle orientation, absolute hand, and contrast loss in single-particle electron cryomicroscopy. *J Mol Biol* 333(4):721–745.
15 Henderson R, et al. (2011) Tilt-pair analysis of images from a range of different specimens in single-particle electron cryomicroscopy. *J Mol Biol* 413(5):1028–1046.
16 Scheres SH (2012) RELION: Implementation of a Bayesian approach to cryo-EM structure determination. *J Struct Biol* 180(3):519–530.
17 Grigorieff N (2000) Resolution measurement in structures derived from single particles. *Acta Crystallogr D Biol Crystallogr* 56(Pt 10):1270–1277.
18 Scheres SHW, Chen S (2012) Prevention of overfitting in cryo-EM structure determination. *Nat Methods* 9(9):853–854.
19 Liu J, Bartesaghi A, Borgnia MJ, Sapiro G, Subramaniam S (2008) Molecular architecture of native HIV-1 gp120 trimers. *Nature* 455(7209):109–113.
20 Tran EE, et al. (2012) Structural mechanism of trimeric HIV-1 envelope glycoprotein activation. *PLoS Pathog* 8(7):e1002797.
21 Meyerson JR, et al. (2013) Molecular structures of trimeric HIV-1 Env in complex with small antibody derivatives. *Proc Natl Acad Sci USA* 110(2):513–518.
22 Huang CC, et al. (2005) Structure of a V3-containing HIV-1 gp120 core. *Science* 310(5750):1025–1028.
23 Scheres SHW, Núñez-Ramírez R, Sorzano COS, Carazo JM, Marabini R (2008) Image processing for electron microscopy single-particle analysis using XMIPP. *Nat Protoc* 3(6):977–990.

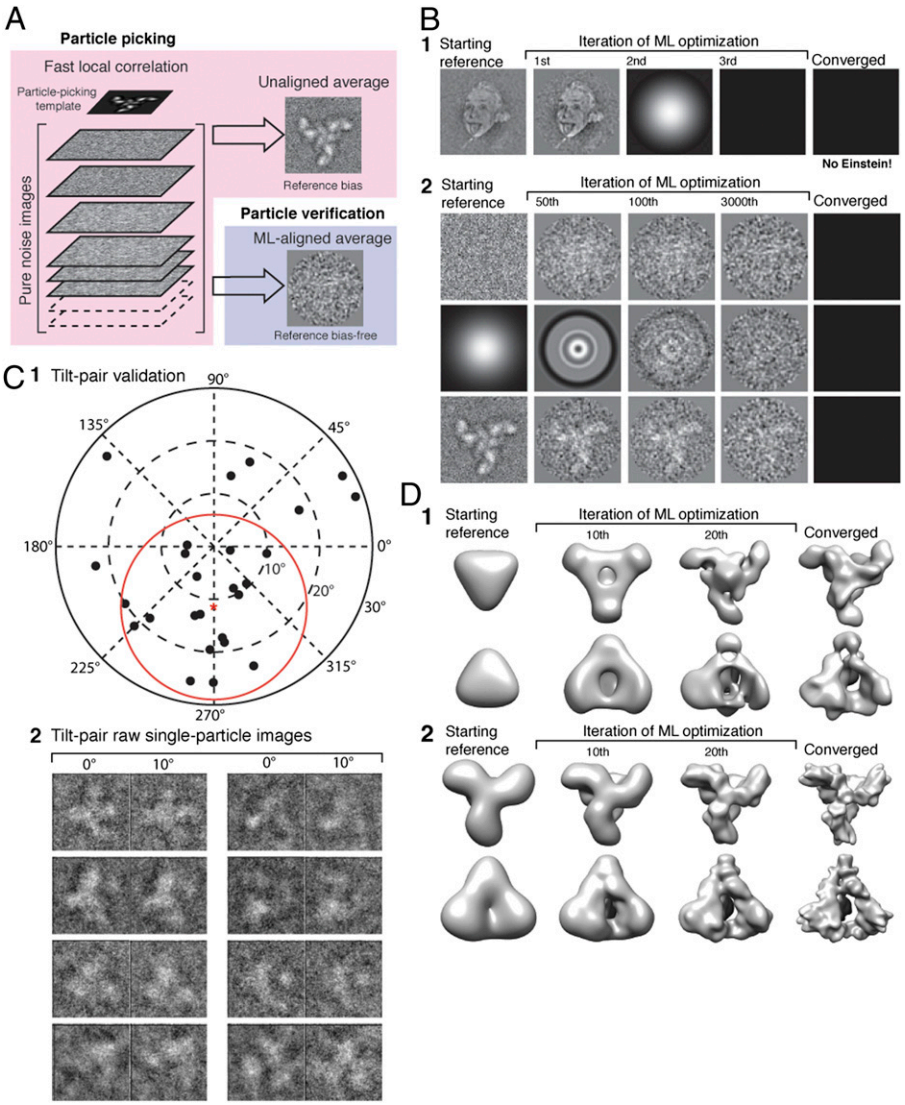

Fig. 1. Validity of the HIV-1 Env(-)ΔCT structure. (*A*) In the dual-target function approach, particles of Env(-)ΔCT trimers are picked by fast local correlation (target function 1) with a low-resolution template. The picked particles are verified by ML alignment, which uses a log-likelihood function (target function 2). Even when the fast local correlation aligns pure noise images to produce an unaligned average image resembling the particle-picking template (reference bias), the ML alignment evaluates the picked particles by optimizing a different target function and removes the reference-biased artifactual feature (6). (*B*) ML alignment is resistant to bias from the starting reference and from the particle-picking template. The head of Einstein starting reference is rapidly removed by a few iterations of ML refinement of the average of 4,485 pure-noise images (*panel 1*). In the experiments shown in panel 2, a single projection of the HIV-1 envelope glycoprotein trimer was used to pick 4,485 "particles" from 200 pure noise micrographs of 4,096 × 4,096 pixels. The picked particles were subjected to ML alignment, using a starting reference of a pure noise image randomly chosen from the particle set (*Top*), a Gaussian circle (*Middle*), or the average of the picked particles without any further alignment (*Bottom*). This starting reference for ML optimization is shown in the first column. Each row shows the history of the ML-aligned averages at the indicated iterations of optimization, ending with the converged average in the far right column. In no case did the particle-picking template appear in the converged ML-aligned averages. (*C*) Tilt-pair raw cryo-EM images of the Env(-)ΔCT trimer were collected at experimental tilt angles of 0° and 10° and a tilt axis of 270° (*panel 2*) with a dose of ~20 electron/Å^2 in each exposure at 80 kV. The tilt-pair parameter plot is shown in *panel 1*, with each tilt pair of particles represented by a point. The radial value indicates the calculated tilt angle, whereas the azimuthal angle indicates the tilt axis. The cluster is indicated by a red circle, whose center is located at the mean tilt angle and axis. (*D*) Two RELION reconstructions were carried out on two independent datasets of the Env(-)ΔCT trimer. In *panel 1*, a 100-Å tetrahedron-like shape was used as a starting reference to refine the Env(-)ΔCT structure with a 9,993-particle dataset; the refinement converged at ~20 Å. In *panel 2*, a low-pass-filtered 60-Å reference was used as a starting reference to refine the structure with a dataset of 124,478 particles; the refinement converged at 10 Å. No mask was used in the RELION refinement. Both RELION reconstructions are compatible with the published 11- and 6-Å Env(-)ΔCT structures (4, 5).

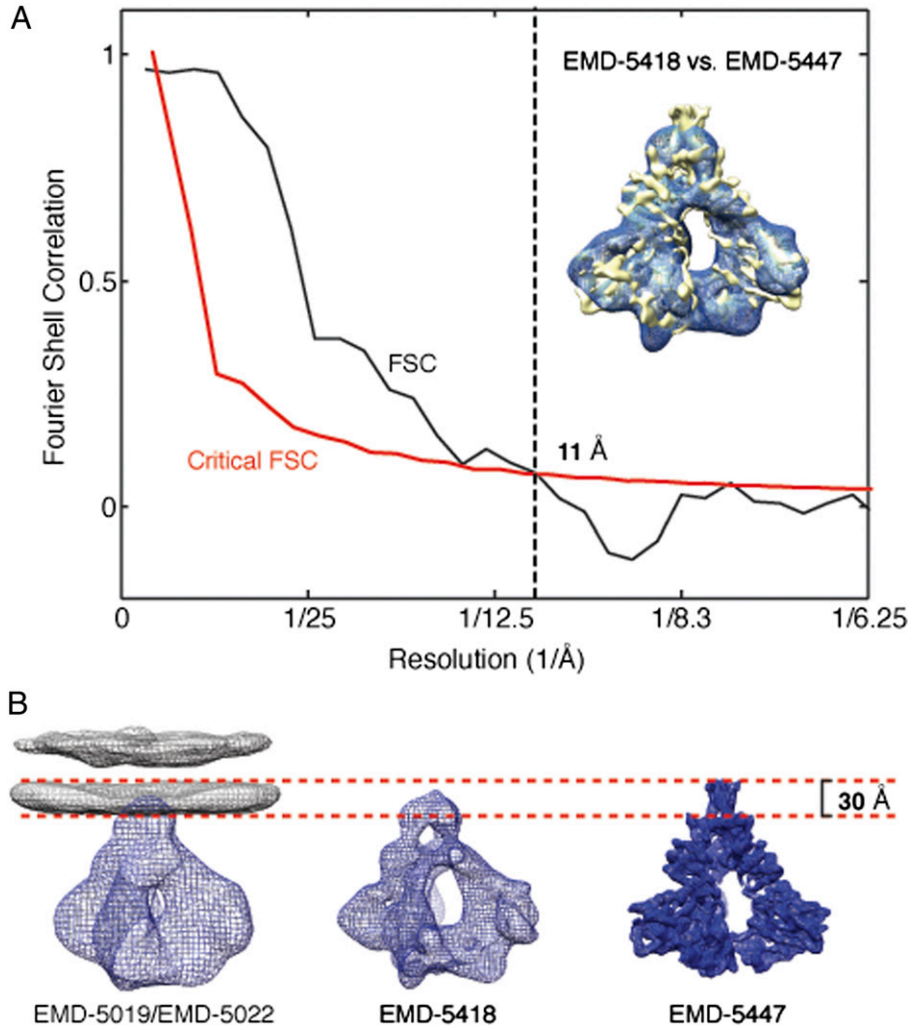

Fig. 2. Comparison of cryo-EM density maps. (*A*) The FSC between the 11-Å map (EMD-5418) (4) and the 6-Å map (EMD-5447) (5) of the Env(-)ΔCT trimer is shown, with the critical FSC calculated from the two maps indicated by the red curve. The FSC curve crosses the critical FSC at ∼11 Å. The alignment of EMD-5418 (blue) and EMD-5447 (yellow) is shown in the *Inset*. The two maps are consistent, with more detailed features in the 6-Å map, as expected. (*B*) The map (EMD-5019) derived by cryo-electron tomography of the native, mature HIV-1 virion spike (19) is aligned with the 11- and 6-Å Env(-)ΔCT maps (EMD-5418 and EMD-5447, respectively) (4, 5). The reported location of the lipid bilayer membrane (EMD-5022) (19) with respect to the tomogram is shown as a gray mesh, with a 30-Å hydrophobic portion of the membrane indicated by the broken red lines. Except for differences in resolution, the three maps are closely related.